colloids and interfaces

MDPI

Article

$Gd(OH)_3$ as Modifier of Iron Oxide Nanoparticles—Insights on the Synthesis, Characterization and Stability

María Gabriela Montiel Schneider [1,*], Paula Sofía Rivero [1], Guillermo Arturo Muñoz Medina [2], Francisco H. Sanchez [2] and Verónica Leticia Lassalle [1]

[1] INQUISUR, Departamento de Química, Universidad Nacional del Sur (UNS)-CONICET, Av. Alem 1253, Bahía Blanca 8000, Argentina
[2] Instituto de Física La Plata IFLP-CONICET, Departamento de Física, Universidad Nacional de La Plata, La Plata 1900, Argentina
* Correspondence: gabriela.montiel@uns.edu.ar

Abstract: Magnetic resonance imaging is one of the most widely used diagnostic techniques, since it is non-invasive and provides high spatial resolution. Contrast agents (CAs) are usually required to improve the contrast capability. CAs can be classified as T1 (or positive) or T2 (or negative) contrast agents. Nowadays, gadolinium chelates (which generate T1 contrast) are the most used in clinical settings. However, the use of these chelates presents some drawbacks associated with their toxicity. Iron oxide magnetic nanoparticles (MNPs) have been extensively investigated as CA for MRI, especially for their capacity to generate negative contrast. The need for more efficient and safer contrast agents has focused investigations on the development of dual CAs, i.e., CAs that can generate both positive and negative contrast with a single administration. In this sense, nanotechnology appears as an attractive tool to achieve this goal. Nanoparticles can be modified not only to improve the contrast ability of the current CAs but also to enhance their biocompatibility, resolving toxicity issues. With the aim of contributing to the field of development of dual T1/T2 contrast agents for MRI, here, we present the obtained results of the synthesis of hybrid nanoparticles composed of magnetite/maghemite and gadolinium hydroxide. Exhaustive characterization work was conducted in order to understand how the hybrid nanoparticles were formed. The nanoparticles were extensively characterized through FTIR and UV–Vis spectroscopy, TEM and SEM microscopy, X-ray diffraction (XRD) analysis, dynamic light scattering, zeta potential, thermogravimetric analysis, energy-dispersive X-ray and vibrating-sample magnetometry. Stabilization studies were carried out to get an idea of the behavior of nanohybrids in physiological media. Special interest was given to the evaluation of Gd^{3+} leaching. It was found that carbohydrate coating as well as the adsorption of proteins on the surface may improve the stabilization of hybrid nanoparticles.

Keywords: iron oxide magnetic nanoparticles; gadolinium hydroxide; hybrid nanoparticles

Citation: Montiel Schneider, M.G.; Rivero, P.S.; Muñoz Medina, G.A.; Sanchez, F.H.; Lassalle, V.L. $Gd(OH)_3$ as Modifier of Iron Oxide Nanoparticles—Insights on the Synthesis, Characterization and Stability. *Colloids Interfaces* **2023**, *7*, 8. https://doi.org/10.3390/colloids7010008

Academic Editor: Reinhard Miller

Received: 7 October 2022
Revised: 7 January 2023
Accepted: 13 January 2023
Published: 17 January 2023

1. Introduction

Magnetic resonance imaging (MRI) is a powerful diagnostic technique, which is characterized by being non-invasive, radiation-free, with a high penetration depth and spatial resolution [1]. Usually, contrast agents (CA) are required to improve the efficiency of the technique. CAs are classified into T1, or positive, and T2, or negative, contrast agents. The former provide brilliant images from the region they are delivered to, while T2 agents provide dark images from the accumulation region [2].

Currently, T1 agents based on gadolinium chelates are the most widely used. However, their use presents some drawbacks associated with their toxicity. For example, they cannot be administrated to patients with chronic renal disease because of the risk of nephrogenic systemic fibrosis [3]. The deposition of gadolinium in the brain and bones even in patients with normal renal function has been reported. There are concerns about the potential harms

of this long-term accumulation [4]. Moreover, gadolinium chelates have low relaxivity (just a few percent of the theoretical potential), so relatively high doses are required to achieve satisfactory contrast [5]. In recent years, the development of gadolinium nanoparticles, especially gadolinium oxide, as CA for MRI has attracted great attention. Nanotechnology emerged as an important tool to improve the stability and biocompatibility of Gd-based CAs. Moreover, higher image contrast can be obtained, since Gd nanoparticles can accumulate in the target tissue, unlike the chelates [6]. Dai MD and co-workers evaluated the in vivo performance of pegylated Gd_2O_3 nanoparticles and the commercial Gd chelate Magnevist. The authors reported that the nanoparticles showed better contrast enhancement in tumors as well as less effect on hepatic and renal function when comparing their performance with Magnevist [7].

On the other hand, magnetic iron oxide nanoparticles (MNPs) have been extensively studied as contrast agents for MRI [8–10]. MNPs can provide negative contrast, and some formulations have been used in clinical settings, although most of them have been withdrawn from the market [11]. However, their non-toxic and biodegradable nature makes them attractive alternatives to the currently available CAs. Both gadolinium-based CAs and magnetic iron oxide are mostly used in only one diagnosis mode (T1 or T2) [12]. The need for more efficient and safer contrast agents has focused investigations on the development of dual CAs. By combining both modalities in a single contrast agent, highly accurate diagnostic information could be obtained. The brilliant or dark images that T1 and T2 CAs provide can also stem from endogenous factors, such as fat or blood clots, making the identification of the signal coming from the contrast agents difficult. Dual T1–T2 CAs could overcome this limitation by providing complementary information in both imaging modalities, allowing a self-confirmation of the signals from the CA [13]. In this context, several dual nanoparticles have been synthesized. For example, Duan et al. prepared a carbon-encapsulated magnetite, which was posteriorly modified with MnO_2. Manganese can provide T1 contrast. In this way, the authors obtained a pH-activable T1–T2* dual CA. A simultaneous enhancement in both T1 and T2* contrast in vivo was detected, improving the differentiation between normal and tumoral tissues [14]. More recently, Bao and co-workers prepared nanorings of magnetite coated with PEI and modified them with gadolinium oxide. This nanosystem not only showed the capacity to act as a dual CA but also demonstrated antitumor effects through hyperthermia treatment [15].

After a survey of the literature, a few contributions were detected concerning the design of nanosystems composed of a magnetic iron oxide and a gadolinium compound. Hence, a lack of rigorous knowledge was detected regarding the synthetic pathways and properties of these kinds of nanosystems. This article is devoted to contributing to this field by proposing the synthesis of a couple of bi-component nanosystems composed of a magnetic iron oxide and gadolinium hydroxide. To this end, a hydrothermal method was used for the synthesis of the iron oxide–PEG formulation (MNPs-PEG) and also to induce Gd coupling. In this way, a nanosystem of MNPs-$Gd(OH)_3$ was formed. Moreover, $Gd(OH)_3$ nanoparticles were synthesized for comparative ends, following the same procedure. Previous articles demonstrated that gadolinium hydroxide nanorods have excellent paramagnetic properties and generate better T1 contrast than the Gd–DTPA complex [16]. The administration of $Gd(OH)_3$ nanorods to mice did not show overt toxicity, validating the use of them in long-term in vivo imaging [17].

Since the leaching of Gd^{3+} could be responsible for the toxicity ascribed to actual Gd-based CA, a strategy to minimize the risk of gadolinium release was devised. Mannose coating was implemented, and stability assays in terms of Gd^{3+} release in simulating physiological media were carried out. The results reported here correspond to the first steps related to the design of dual CAs for MRI, where a rigorous study and understanding of the synthetic pathways, mechanisms and properties of hybrid nanosystems are required for the later validation of their ability as CA in MRI assays, as performed in our previous works [18].

2. Materials and Methods

2.1. Materials

All reagents were of analytical grade and used without further purification. Ferric chloride hexahydrate was purchased from Tetrahedron (Argentina). Ferrous sulphate heptahydrate was provided by Mallinckradt Chemical Works (USA). Polyethylene glycol (PEG 6000) was acquired from Biopack (Argentina). Gadolinium nitrate hexahydrate and mannose were purchased from Sigma Aldrich (USA). Sodium hydroxide was provided by Cicarelli (Argentina). Fetal bovine serum was acquired from Internegocios S.A (Argentina). A standard solution of gadolinium 1000 ppm was provided by Carlo Erba.

2.2. Methods

2.2.1. Synthesis of Mag@PEG

Magnetic nanoparticles were synthesized by the hydrothermal method. PEG 6000 (0.5965 g) was dissolved in 30 mL of distilled water. Afterward, iron salts were added to the solution (0.6687 g of Fe^{3+} salt and 0.3607 g of Fe^{2+}). After 10 min of stirring at room temperature, a solution of NaOH 5M was added until the pH reached a value higher than 10. The reaction mixture was placed into a Teflon-lined autoclave and kept in an oven at 160 °C for 9 h. Then, it was allowed to cool to room temperature. The nanoparticles were decanted over a neodymium magnet, and the supernatant was removed. Nanoparticles were washed with distilled water until the pH and conductivity reached values close to those of distilled water.

2.2.2. Synthesis of $Gd(OH)_3$ Nps

Gadolinium nitrate hexahydrate (0.1180 g) was dissolved in 50 mL of distilled water. The solution was stirred for 1 h at 25 °C, and then, a solution of NaOH 5M was added. The reaction mixture was stirred for another hour and then placed into a Teflon-lined autoclave. The mixture was kept in the oven at 160 °C for 20 h and then cooled to room temperature. Nanoparticles were centrifuged and washed with distilled water until the pH and conductivity reached levels roughly comparable with those corresponding to distilled water.

2.2.3. Synthesis of Mag@$Gd(OH)_3$

An amount of Mag@PEG (83 mg) was dispersed in 50 mL of distilled water under sonication. Then, the dispersion was magnetically stirred, and 117 mg of $Gd(OH)_3$ was added in one portion. The reaction mixture was stirred at 25 °C for 1 h. Afterward, a solution of NaOH 5M was added until the resulting pH was higher than 10. Subsequently, the mixture was placed in a Teflon-lined autoclave and heated at 160 °C for 20 h. The purification process was performed exactly as for Mag@PEG.

2.2.4. Influence of the Biological Media: Interaction with Proteins

Mag@$Gd(OH)_3$ was dispersed in 5 mL of buffer phosphate (PBS) under sonication. Then, 40 mL of fetal bovine serum (FBS) was added, and the mixture was kept at 37 °C for 1 h. It has been reported that this time is enough to form a stable protein corona around nanoparticles [19]. The nanoparticles were magnetically decanted and washed, as explained before in Section 2.2.1.

2.2.5. Mannose Coating Procedure: Mag@$Gd(OH)_3$@Man

An amount of Mag@$Gd(OH)_3$ (52.7 mg) was dissolved in 40 mL of distilled water under sonication for 30 min. Then, 0.66 mL of a 20% mannose solution was added. The reaction mixture was stirred at room temperature for 19 h. Afterward, the nanoparticles were washed with distilled water, as indicated in Section 2.2.1.

2.2.6. Stability Assays

The stability assay was carried out with Mag@$Gd(OH)_3$ and Mag@$Gd(OH)_3$@Man. Amounts of these nanosystems were dispersed in 50 mL of PBS. The reaction mixture was magnetically stirred for 24 h at 37 °C. At certain times, the mixture was placed on a neodymium magnet, and aliquots were taken and analyzed under UV–Vis spectroscopy. Finally, the nanoparticles were washed and dried.

2.3. Characterization Methods

Fourier transform spectroscopy (FTIR) spectra were recorded in a Thermos Scientific Nicolet iS50 in the frequency range of 400–4000 cm^{-1} using the KBr pellet method. Transmission electron microscopy (TEM, JEOL 100 CX II, Tokyo, Japan) operating at 100 KeV and a resolution of 2 nm was used to determine the size and morphology of the particles. Samples were dissolved in water, placed on 200 mesh Cu grids and dried to room temperature. Morphology was also studied by scanning electron microscopy (SEM) using a LEO EVO 40 XVP scanning electron microscope, with a secondary electron detector. The observation was made at 10 KV. With an Oxford X-max 50 energy-dispersive X-ray microanalysis system (EDS) attached to the microscope, a microanalysis of elemental chemical composition of a defined area of the sample was performed. The energy-dispersive microanalysis system allows the identification of elements from Lithium (Z = 3). Its detection limit is 0.1% by weight for elements with an atomic number greater than aluminum and 0.5% by weight for light elements. An Argon plasma metallizer Sputter coater 91000, PELCO brand, Model 3. Ted Pella Inc. was used to metallize the samples with Au.

UV–Vis spectroscopic measurements were carried out using a spectrophotometer (Shimadzu 160 Japan).

The X-ray diffraction (XRD) pattern of the nanoparticles was recorded in a PANalytical Empyrean 3 diffractometer with a Ni filtered CuKα radiation, a graphite monochromator (in the case of samples containing iron) and a PIXcel3D detector. It was operated at a voltage of 45 kV and a current of 40 mA, in the 2θ range from 10° to 80°, using a continuous scanning mode with an angular scanning speed of 0.016° min^{-1}.

Thermogravimetric analysis (TG) was performed using TA Q600 equipment. Samples were weighted (between 20 and 30 mg) and heated at room temperature up to 800 °C at a rate of about 10 °C/min under an air atmosphere.

The iron content was measured by atomic absorption spectroscopy using GBC Avanta 932 equipment. Gadolinium content was determined by inductively coupled plasma atomic emission spectrometer (ICP) Shimadzu Sequential 1000 S (λ 342.24 nm), according to the EPA standard 200.7. An external calibration methodology was performed with a standard solution of gadolinium 1000 pm (Carlo Erba) and ultra-purified nitric acid.

Data on the hydrodynamic diameter and Z potential (ζ) were acquired using a Malvern Zetasizer (Nano-Zs90). Samples were dispersed in distilled water and sonicated between 30 to 60 min before performing the acquisition.

The magnetization cycles of the samples were measured at room temperature with a Lakeshore 7404 VSM at an oscillation frequency of 82 Hz and amplitude of 5 mm. The airgap was set at 20 mm, and the applied field was varied at $\pm$1.9 T.

3. Results

3.1. Synthesis of Hybrid Nanosystems

In order to obtain a hybrid iron-oxide–gadolinium nanosystem, the iron oxide core was first prepared using PEG as a stabilizer. Black iron oxide nanoparticles were obtained after hydrothermal treatment. The yield obtained was almost 53.9% of the expected mass. These nanoparticles were used as a nanoplatform base for the subsequent treatment with gadolinium nitrate. A further hydrothermal treatment was performed, yielding a brown precipitate identified as Mag@$Gd(OH)_3$. The yield of the hybrid nanoparticles was almost 36.5% of the theoretical mass. The same experiment was carried out without the addition of Mag@PEG, as described in the Materials and Methods section. In this case, $Gd(OH)_3$

Nps were obtained after heating in an oven. The percentage of nanoparticles obtained was 65.8% with respect to the theoretical mass.

3.2. Characterization of Raw and Hybrid Nanosystems Mag@Gd(OH)$_3$

The three synthesized nanosystems were fully characterized in order to elucidate the kinds of interactions between the magnetic phase and Gd in the hybrid nanosystem Mag@Gd(OH)$_3$.

- Crystalline Pattern by XRD

Figure 1 shows the diffractogram of the three nanosystems. For Mag@PEG, the characteristic diffraction peaks of magnetite/maghemite iron oxides were observed. The typical crystalline pattern is compatible with the presence of signals at 2θ = 30.1°, 35.4° and 62.6°, which are associated with the planes (220), (311) and (440), respectively. On the other hand, it was found that for gadolinium nanoparticles, the diffractions peaks matched with those corresponding to Gd(OH)$_3$. The most important peaks are found at 2θ = 16.2°, 28.2° and 29.5°, which correspond to the (100), (110) and (101) planes of the hexagonal phase, respectively [20]. Finally, the diffractogram of Mag@Gd(OH)$_3$ shows peaks related to the above-mentioned crystalline pattern, i.e., magnetite/maghemite and Gd(OH)$_3$. It is worth mentioning that in the case of Mag@PEG and Mag@Gd(OH)$_3$, the XRD data are not sufficient to discern whether the magnetic phase is maghemite or magnetite. Hence, it is correct to refer to it as the magnetic iron oxide phase.

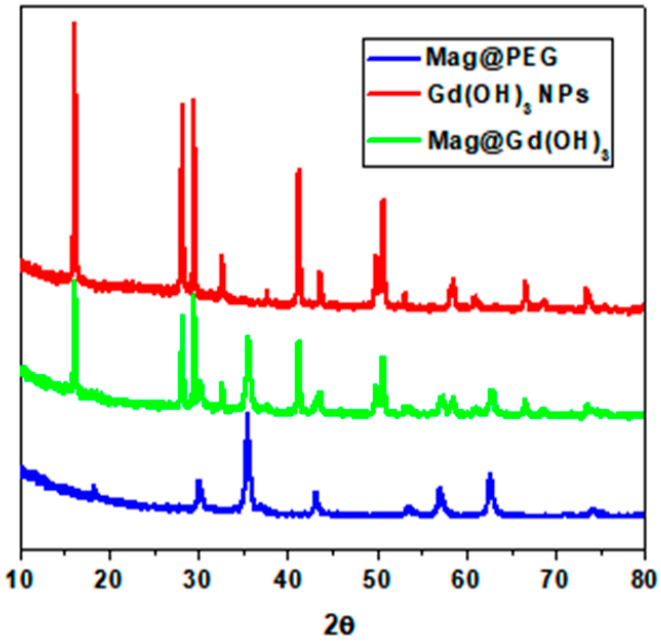

Figure 1. Comparative XRD diffractograms of the raw and hybrid nanoparticles.

The Scherrer equation allows the calculation of the crystal size, taking into account the width of the dominant peak. In the case of Mag@PEG, the crystal core is 20 nm. For Mag@Gd(OH)$_3$, the main peak seems to be 2θ = 35.5°, corresponding to the magnetic iron oxide, so the size of the crystal core can be estimated as 23 nm.

- FTIR and UV–Vis Spectroscopy

Figure 2a shows the FTIR spectra of the synthesized hybrid nanoparticles as well as the raw nanoparticles. For Mag@PEG, the characteristic peaks associated with the stretching vibration of the Fe–O bond at 582 cm^{-1} can be seen. On the other hand, the bands associated with the polymer assigned to methyl and methylene groups are barely distinguished at 2919 and 2852 cm^{-1}.

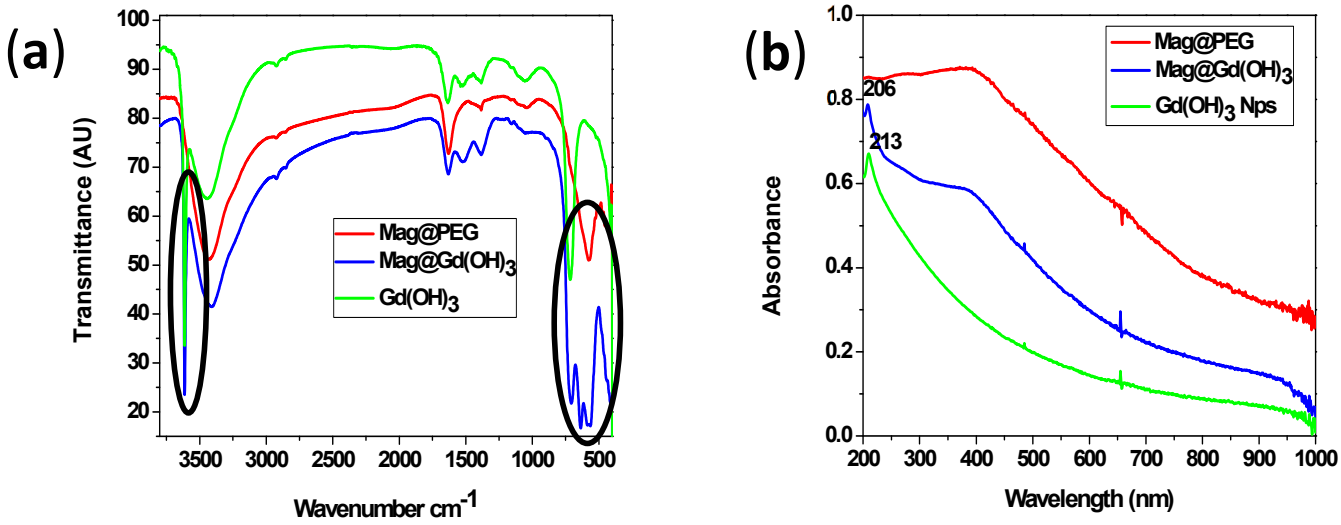

Figure 2. (**a**) FTIR spectra of the three nanosystems. The regions that reveal the presence of both $Gd(OH)_3$ and maghemite are marked. (**b**) UV–Vis spectra of the nanoparticles.

In the FTIR spectrum of $Gd(OH)_3$ NPs, the stretching and bending bands associated with the Gd–OH bond at 3612 and 714 cm^{-1} (a sharp band), respectively, are clearly distinguished [20]. The small adsorption band at 1635 cm^{-1} could be attributable to the molecules of H_2O physically adsorbed on the surface [21]. The FTIR spectrum of $Mag@Gd(OH)_3$ shows the bands of Gd-OH at 3612 and 706 cm^{-1} as well as the band of the Fe-O vibration at 564 cm^{-1}. Moreover, a new band at 636 cm^{-1} appears. This band reveals the presence of maghemite [22], which is possible as a consequence of the oxidation of magnetite during the second hydrothermal treatment. Based on these data, it can be said that the presence of maghemite is more important in $Mag@Gd(OH)_3$ than in Mag@PEG.

UV–Vis spectroscopy also allows the identification of the gadolinium phase in $Mag@Gd(OH)_3$ by comparison with the UV characterization of $Gd(OH)_3$ (Figure 2b). A small sharp peak at 213 and 206 nm for $Gd(OH)_3$ NPs and $Mag@Gd(OH)_3$, respectively, reveals the presence of gadolinium hydroxide [23].

- Transmission Electron Microscopy (TEM) and Scanning Electron Microscope (SEM)

TEM micrographs show the morphology and size of the nanoparticles (Figure 3). In the case of Mag@PEG, the observed morphology is predominantly cubic, with a size of about 23.5 nm. This size is correlated with the one calculated from the Scherrer equation. For $Gd(OH)_3$ NPs, the transmission electron microscopy reveals that they are actually nanorods in shape. In this case, the length and the width of the nanorods were determined, with an average value of 54 nm for the width and an average of 310 nm for the length. The micrograph of $Mag@Gd(OH)_3$ shows a heterogeneous morphology combining cubic and rod particles.

The first impression could be that the nanohybrid system was a mixture of Mag@PEG and $Gd(OH)_3$ Nps instead of hybrid nanoparticles. To determine whether $Mag@Gd(OH)_3$ was formed by hybrid nanoparticles or not, a physical mixture of Mag@PEG and $Gd(OH)_3$ was prepared by mixing them in a mortar. Then, both, $Mag@Gd(OH)_3$ and the physical mixture were analyzed by SEM microscopy. Figure 4 shows that the morphological differences between the two samples are considerable. As the differences in SEM images are remarkable, it could be concluded that $Mag@Gd(OH)_3$ is a hybrid system, where the gadolinium phase is interacting with the magnetic iron oxide.

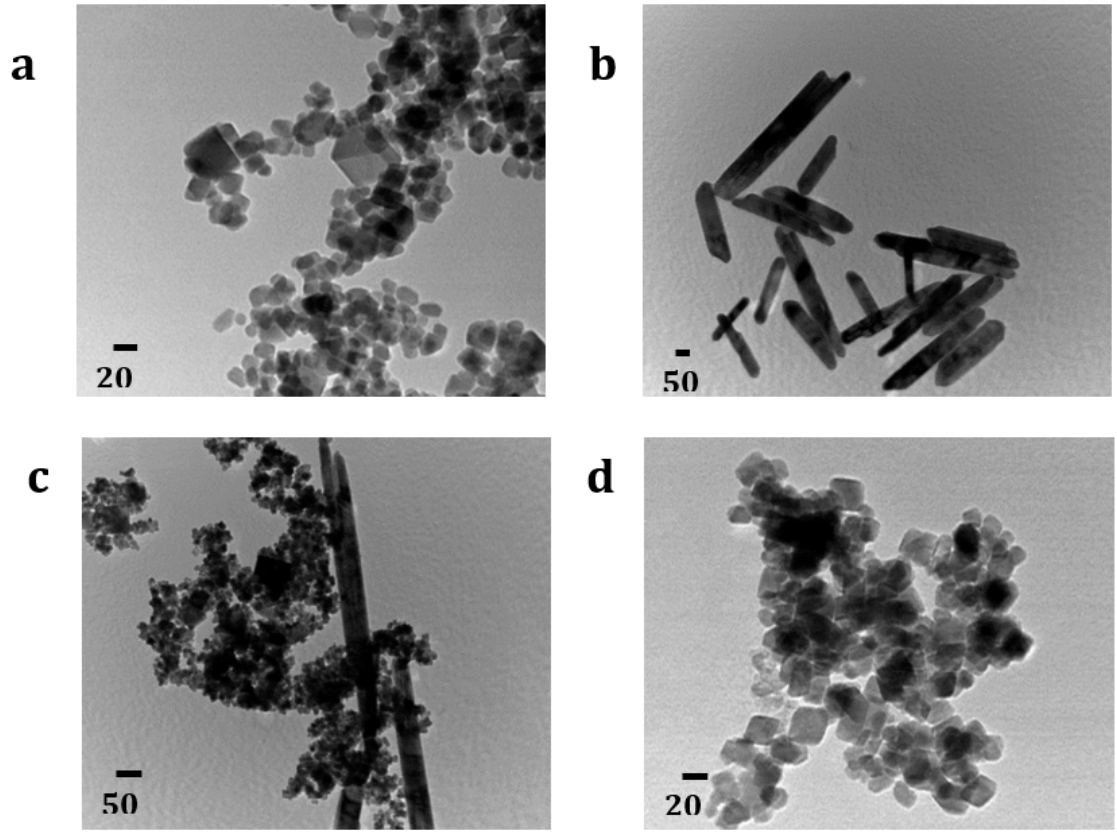

Figure 3. TEM micrographs of (**a**) Mag@PEG, (**b**) $Gd(OH)_3$ Nps, (**c**) and (**d**) Mag@$Gd(OH)_3$.

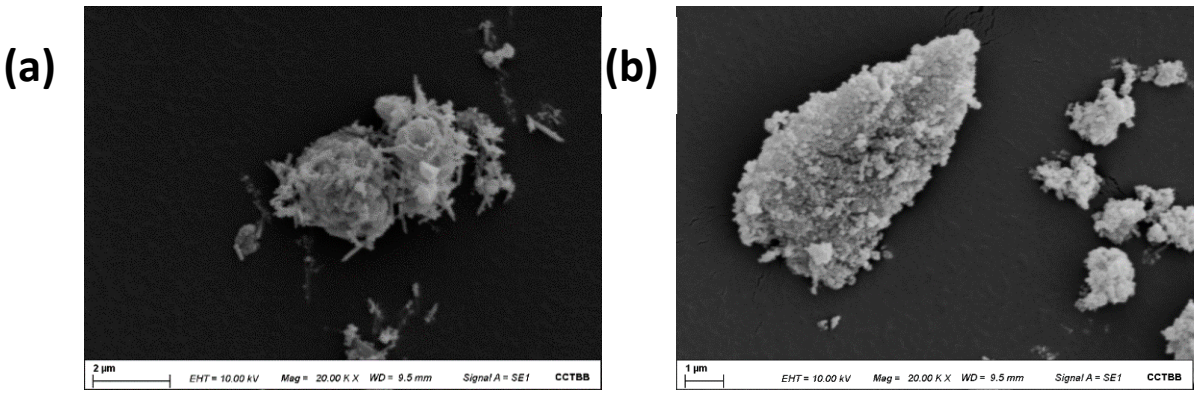

Figure 4. (**a**) SEM image of Mag@$Gd(OH)_3$. (**b**) SEM image of a physical mixture of Mag@PEG and $Gd(OH)_3$ Nps.

- Hydrodynamic Diameter

The chemical and physical properties of the nanoparticles are strongly linked to their size and size distribution. The smaller they are, the more exposed their surface is [24]. This means that the size of nanoparticles restricts their applications, especially in the field of nanomedicine. Nanoparticles intended for biomedical purposes should have a hydrodynamic diameter between 10 and 300 nm, and they have to be monodisperse [25]. The size distribution population of a given sample is represented by the polydispersity index (PDI). For monodisperse nanoparticles, the PDI values are found between 0.01 and up to 0.7. Higher values indicate a broad size distribution [26]. Table 1 shows the size and size distributions for the three nanosystems measured in water at a nanoparticle concentration of 0.1 mg/mL.

Table 1. Hydrodynamic diameter and zeta potential of Mag@PEG, $Gd(OH)_3$ Nps and Mag@$Gd(OH)_3$.

	Hydrodynamic Diameter (nm)	PDI	Zeta Potential (meV)
Mag@PEG	208.8 ± 6.6	0.473	−25.6
$Gd(OH)_3$ Nps	243	0.045	−17.2
Mag@$Gd(OH)_3$	264.6 ± 2.8	0.328	−33.5

All samples are monodisperse, according to the PDI values, which are lower than 0.7 for the three. A slight increase in HD was seen in Mag@$Gd(OH)_3$ compared with Mag@PEG. Moreover, the nanohybrid system shows a high negative zeta potential. The numerous OH^- groups around Mag@$Gd(OH)_3$ could be responsible for this value [21].

- Energy-Dispersive X-ray (SEM-EDS)

The energy-dispersive X-ray (EDX) enables the chemical characterization of a sample. The elemental mapping (which shows the chemical distribution) and line scanning (a chemical analysis along a horizontal line) of Mag@$Gd(OH)_3$ reveal that the sample is composed of iron, gadolinium and oxygen. Figure 5 shows the spectra of Mag@$Gd(OH)_3$. Gold is present because it is used as a metallizer to make the sample conductive. Similarly, the detection of significant amounts of carbon could arise from the glue of the aluminum single-side tape, which is used in the sample holder. Figure 5 shows a general spectrum of hybrid nanoparticles.

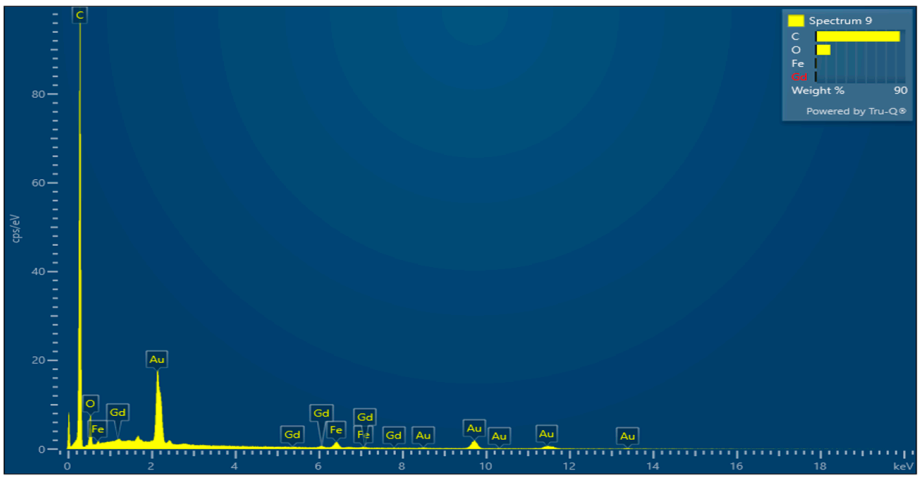

Figure 5. SEM-EDS spectra of Mag@$Gd(OH)_3$. The high C detection did not come from the nanoparticles (see main text).

Iron is found in a higher proportion than gadolinium, which means that iron oxide is the predominant phase in hybrid nanoparticles. Figure 6a shows the elemental mapping, where the distribution of the different elements, i.e., Fe, Gd and O, can be seen. It is observed that Fe and Gd are homogeneously distributed all along the analyzed clusters. It is worth mentioning that segregated fractions of pure gadolinium hydroxide or iron oxide are not observed in the analized region. To further support these data, the same sample was evaluated with a line scan (Figure 6b). The intensity of the signal can be directly related to the amount of each element in the analyzed region. It is observed that the intensity of iron and oxygen increased on the center of the NPs cluster. On the other hand, gadolinium seems not to follow the same tendency, and its intensity appears to be slightly more pronounced on the edge of the cluster.

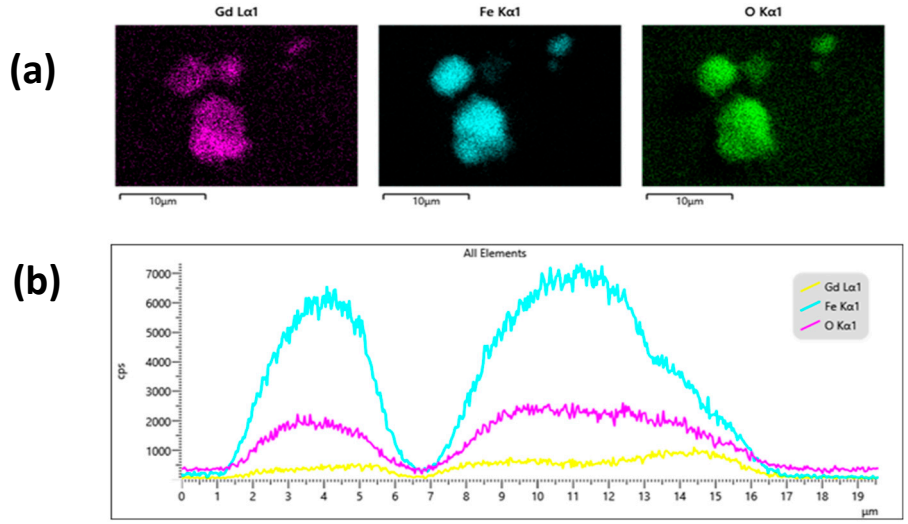

Figure 6. (**a**) Elemental mapping of the elements found in Mag@$Gd(OH)_3$. (**b**) Line scan showing the distribution of the elements along a line over a determined region.

- Thermogravimetric Analysis

The sample's composition was also evaluated through thermogravimetric analysis. Figure 7 shows the TG and DSC curves of the raw and hybrid materials. The TG curve of Mag@PEG shows an initial weight loss between room temperature and 175 °C, which is related to surface water desorption. It has been reported that magnetite experiences an exothermic process with mass gain between 100 and 190 °C due to the oxidation of Fe_3O_4 to γ-Fe_2O_3. However, the endothermic process due to water desorption, which occurs before this transformation, may overlap it [22]. The weight loss that takes place between 180 and 470 °C may be related to the decomposition of PEG [27]. This fraction corresponds to 2.88% of the total weight. Finally, the DSC curve shows an exothermic process at 602 °C. This process takes place without mass change and can be associated with the oxidation of γ-Fe_2O_3 to σ-Fe_2O_3 [28].

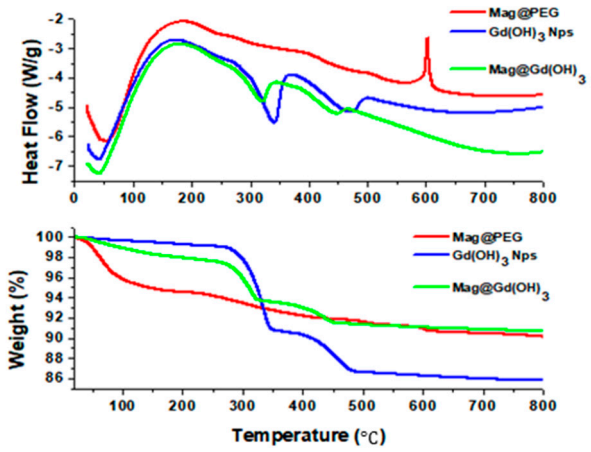

Figure 7. DSC (**top**) and TG (**bottom**) curves of the raw and hybrid nanoparticles.

The DSC/TG curves of $Gd(OH)_3$ Nps show a gradual weight loss between room temperature and 230 °C, which corresponds to surface water desorption. Gadolinium hydroxide dehydrates to gadolinium oxide. This transformation is observed as a two-step process [29]. First, $Gd(OH)_3$ reacts to GdOOH. This transformation occurs between 300 and 350 °C, with an endothermic peak at 340 °C. The mass loss of this step is 7.85%. In the second step, the intermediate GdOOH dehydrates to Gd_2O_3. This process occurs

between 350 and 430 °C, with an endothermic peak at 469 °C. The mass loss of the last step represents 4.07%.

The TG/DSC curves of Mag@Gd(OH)$_3$ clearly show the endothermic weight changes associated with the oxidation of Gd(OH)$_3$ to Gd_2O_3 but shifting to lower temperatures (321 and 447 °C). In this case, the exothermic transition from maghemite to hematite is not observed. The reason may be due to a protective effect of the gadolinium phase present and the possible interactions generated between them.

- Magnetic Measurements

Figure 8 shows the magnetization curves of Mag@PEG and Mag@Gd(OH)$_3$. Both samples present superparamagnetic behavior, and negligible coercivity is observed. Mag@PEG shows a saturation magnetization value of 58.9 emu/g, while Mag@Gd(OH)$_3$ shows a value of 41.1 emu/g. As FTIR clearly detects the presence of maghemite, part of the reduction in the saturation magnetization of Mag@Gd(OH)$_3$ could be attributable to the possibly higher presence of this iron oxide than in Mag@PEG, as well as to the presence of gadolinium hydroxide, since the value is lower than the one reported for bare maghemite (80 emu/g) [30]. Gd(OH)$_3$ shows the expected paramagnetic behavior.

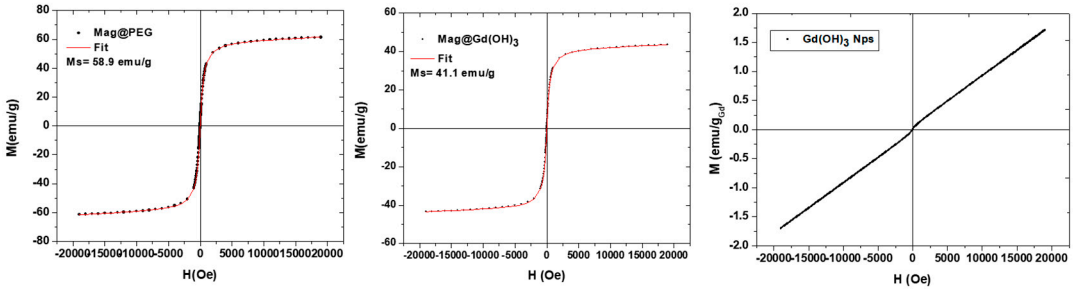

Figure 8. VSM measurements of the raw and hybrid nanomaterials.

The magnetic size determined for Mag@PEG and Mag@Gd(OH)$_3$ was 10 and 11 nm, respectively. These values were obtained by fitting the magnetization curves with the Langevin model, assuming a lognormal distribution of spherical particles. The sizes are lower than those estimated by TEM and the Scherrer equation, which can be considered the real sizes, since it is assumed that there is a magnetically "dead" layer due to the surface magnetic disorder of the particle. For that reason, the magnetic response depends mainly on the ordered atomic moments of the nanoparticle. This behavior has been studied and reported by Muskas et al. [31].

3.3. Influence of the Biological Media: Study on Protein Corona Formation

It is well known that once the nanoparticles ingress into the in vivo environment, they make contact with biological fluids, proteins (and other biomolecules), which rapidly cover the nanoparticles' surface, modifying their physicochemical properties (i.e., size, surface charge, size distribution, etc.) [32].

The influence of these media on surface functionality was mainly analyzed. Therefore, FTIR spectroscopy was assayed and demonstrated the incorporation of proteins on the surface of Mag@Gd(OH)$_3$. The presence of the amide group is noticeable (Figure 9a). An increase in the intensity and shift of the signal at 1646 cm^{-1} of amide band I is observed, associated with the carbonyl function. Amide band II, related mostly to plane bending of N-H, appears around 1540 cm^{-1}. After the treatment with FBS, a band at 1072 assigned to the vibrations of C-COO is detected [33]. Moreover, the region corresponding with the stretching vibrations of O-H is much wider and slightly shifted with respect to the one found in the spectra of the raw hybrid nanoparticles. The bands around 3600 and 700 cm^{-1}, corresponding to the vibration of Gd bonded with O-H, are lower in intensity. This may be a consequence of the presence of proteins interacting with the surface of the nanoparticles, masking the signal of gadolinium hydroxide.

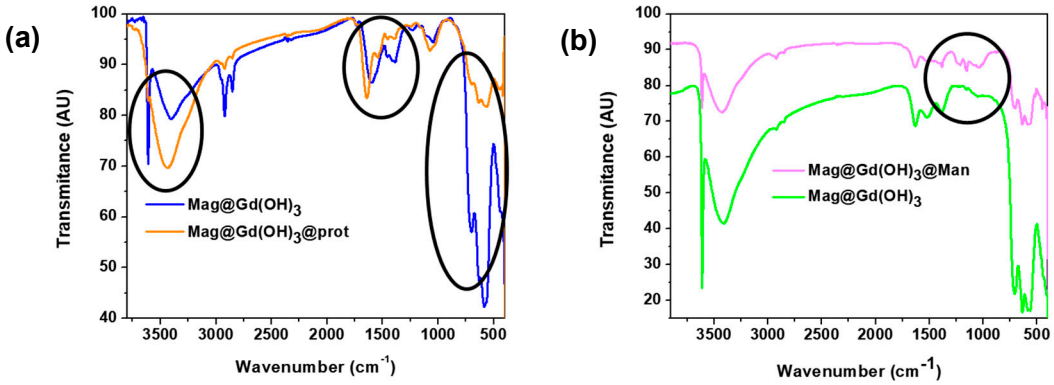

Figure 9. (**a**) Comparison between FTIR of (**a**) Mag@Gd(OH)$_3$ before and after protein adsorption. (**b**) Mannose-coated and uncoated hybrid nanoparticles. In both cases, the areas of interest are marked.

The hydrodynamic diameter was also evaluated after the hybrid nanosystems' incubation in FBS. Protein-modified nanoparticles were dispersed in water under the same conditions as the unmodified ones. It was observed that the particle size increased for Mag@Gd(OH)$_3$ from 264 to 400 nm, which can be considered an indicator of the formation of a protein corona around the nanoparticle. The HD of protein-modified Mag@Gd(OH)$_3$ was measured four months later, and it was found that its value remained almost unaltered, which indicated the high stabilization achieved after protein absorption.

3.4. Surface Modification of Hybrid Mag@Gd(OH)$_3$: Mannose Coating

To increase the hybrid nanosystem's stability in terms of Gd leaching, a further treatment was implemented using mannose as coating. This monosaccharide was chosen, since it was extensively reported that the mannose receptor is overexpressed in different kinds of tumors and in activated macrophages, being involved in the inflammatory process [34].

The incorporation of mannose was achieved following a simple methodology described in the Materials and Methods section. FTIR confirmed the presence of sugar on the surface of the nanoparticles (Figure 9b). The characteristic peaks of C-H at 2900, C-O at 1384–1200 and C-O-C at 1040 are detectable [35].

The HD of the mannose-coated nanoparticles was 386 nm, slightly higher than the uncoated nanoparticles. The increase could be associated with the formation of a mannose coating. A dramatic change in the zeta potential was registered, since it turned positive (+14.5 mV). This may be explained in terms of the pka of mannose, which is 12.1 [36]. Since a determination of the zeta potential was made at pH 6.25, mannose remained protonated. The positive zeta potential in sugar-modified nanoparticles was previously reported [37]. On the basis of the characterization results, a successful mannose surface incorporation can be demonstrated.

Figure S1 (Supplementary Material) shows a TEM image of Mag@Gd@Man. In this micrograph, the presence of iron oxide magnetic nanoparticles attached to the surface of gadolinium hydroxide rods is clearly visible. This image reinforces the idea of the formation of a nanohybrid system composed of iron and gadolinium. The presence of some agglomerates of iron oxide nanoparticles is likewise detectable.

Stability Assays

Stability assays were performed for Mag@Gd(OH)$_3$ and Mag@Gd(OH)$_3$@Man with the aim of determining whether the hybrid nanoparticles could be stable in a medium simulating the physiological environment. Stability was evaluated in terms of the possible leaching of Gd species. Moreover, the intention was to define the role of mannose in such a stabilization process. UV–Vis spectroscopy data demonstrated that Gd^{3+} was released from Mag@Gd(OH)$_3$. Moreover, the concentration of Gd^{3+} increased in a time-dependent manner. Figure S2 (Supplementary Material) shows the UV spectra from aliquots taken at 1, 3, 5 and 24 h.

A different behavior was observed when Mag@Gd(OH)$_3$@Man was studied, since the leaching of the gadolinium ion seemed to be insignificant. Figure S2 shows the UV spectra obtained from aliquots taken at 1, 6 and 24 h. As expected, the presence of mannose seemed to confer more stability to the nanohybrid particulates, since the concentration of leached Gd remained almost constant over the assay period.

To corroborate the stabilizing effect of mannose, the concentration of Gd in the solid remanent nanohybrids was measured by ICP before and after the stability assay. The recorded data are listed in Table 2 and correlate well with the data arising from supernatants measured by UV–visible spectroscopy. These data reinforce the function of mannose as a barrier to prevent Gd^{3+} release. The analysis was complemented by the FTIR analysis of solid nanohybrids, which was consistent with the UV–visible and ICP data (data not shown are included in Supplementary Material, Figure S3).

Table 2. Reduction in gadolinium phase, expressed as mg Gd(OH)$_3$/100 mg of the sample, in Mag@Gd(OH)$_3$ and Mag@Gd(OH)$_3$@Man before and after stability assay in PBS.

	Amount of Gd(OH)$_3$ before Stability Assay *	**Amount of Gd(OH)$_3$ after Stability Assay ***	**% of Gd(OH)$_3$ Reduction**
Mag@Gd(OH)$_3$	40	17.9	55%
Mag@Gd(OH)$_3$@Man	26.9	17.2	36.1%

* expressed as mg Gd(OH)$_3$/100 mg of the sample.

The lower initial amount of Gd(OH)$_3$ in Mag@Gd(OH)$_3$@Man than in Mag@Gd(OH)$_3$ (17.9 and 40%, respectively) may be explained in terms of the presence of an extra component in the total sample mass (mannose).

4. Discussion

As stated earlier, efficient and safer CAs for MRI are considered a necessity for improving the diagnosis. The design of nanotechnological devices as feasible tools is a challenging field of research. They should meet the physicochemical requirements for in vivo administration, including acceptable stability during the period of time circulating in the bloodstream [38]. A further requirement is added concerning the possibility of combining two moieties (gadolinium and iron oxide) able to confer a dual CA character.

Here, the synthesis of hybrid nanoparticles involved the use of previously formed pegylated iron oxide nanoparticles. Polyethylenglicol was chosen because of its hydrophilicity and biocompatibility [39]. From the characterization of Mag@PEG, it can be concluded that the percentage of the polymer present is quite low (around 3%), which is in agreement with previous reports [40].

According to the characterization data of Mag@Gd(OH)$_3$, the interactions apparently occurred at the surface level, involving the amphoteric iron oxide surface and Gd hydroxyl moieties. Even when the interactions remained restricted at the surface level, they were well characterized and verified by data arising from SEM-EDS. Moreover, the data from HD and Z potential reinforced the idea of Gd surface interactions because of the changes noticed with respect to the raw nanosystems.

The information regarding these kinds of nanohybrid materials is limited in the available literature, including the patents. A recent article reported the preparation of hybrid nanoparticles obtained after the modification of iron oxide with gadolinium. The authors obtained a nanocomposite composed of magnetic iron oxide agglomerates surrounded by gadolinium oxide in a core–shell structure [41]. Although the method of synthesis proposed in the mentioned work is quite similar to the one employed in this work, a substantial difference is noted in the final step. While Shabanzadeh-Kouyakhi et al. annealed the sample at 300 °C after the addition of gadolinium salt, in the present work, the mixture of Mag@PEG with gadolinium was placed in a hydrothermal reactor. Thus, gadolinium hydroxide was obtained instead of gadolinium oxide. Moreover, in the present

work, a core–shell structure was not achieved. The hydrothermal treatment mentioned modified the composition of the iron oxide phase, since magnetite was partially oxidized to maghemite. This transformation was clearly detected through FTIR spectroscopy, as mentioned in the Results section. The TG/DSC curves for Mag@Gd(OH)$_3$ did not exhibit the final transformation of maghemite into hematite. It is believed that Gd(OH)$_3$ protects iron oxide from further oxidations. Similar observations were raised by Fajaroh et al. when studying the nanosystem of silica-coated magnetite. The authors observed that after an annealing process, the silica-coated magnetite converted into maghemite, but the transition to hematite did not occur. On the contrary, uncoated magnetite oxidized to hematite. The results may indicate a protective effect of the coating [42]. Although the structure of Mag@Gd(OH)$_3$ probably involves magnetic iron oxide attached to gadolinium hydroxide nanorods, the interaction between the two phases could protect iron oxide from further oxidation processes. In other words, the thermogravimetric analysis gives more evidence on the interaction between the Fe and Gd phases.

XRD shows both the magnetite/maghemite and gadolinium hydroxide phases, revealing the presence of the gadolinium compound and magnetite/maghemite. It is worth mentioning that in the hybrid material, the main peak belongs to the magnetite/maghemite phase. Moreover, if the Scherrer equation is calculated with this peak, the size of the crystal of the magnetic phase does not change Mag@Gd(OH)$_3$. The hybrid nanoparticles preserved the superparamagnetic behavior of the iron oxide core, which was consistent with previous results. The modification of magnetite with paramagnetic manganese dioxide yielded superparamagnetic compounds with lower magnetization to saturation curves due to the presence of paramagnetic material [43].

Considering nanoplatforms for biomedical applications, it is not possible to disregard their behavior in physiological media. Properties such as size, size distribution, surface charge and shape are critical when interactions with the components of the plasma, cell or other biological entities are considered. The formation of a protein layer is the first requirement to minimize the risks to the nanosystems being cleared by the RES, regardless of their size. Therefore, the assays performed tended to demonstrate the ability of hybrid nanosystems to efficiently interact with representative proteins. Moreover, it was seen that proteins stabilized the hybrid nanoparticles, since no change in HD was observed after four months of storage. The improvement in the colloidal stability of magnetic nanoparticles after protein corona formation has been reported earlier [44,45].

In the framework where these nanohybrid systems will be applied, another concern is paramount: the stability in terms of leaching of Gd^{3+}. In this regard, it is important to highlight that, according to the stability assays performed within this work, most gadolinium is lost after 24 h, which is a considerably longer period of time than the time needed for nanoparticles to reach the target tissue. Yang et al. reported that Gd(OH)$_3$ nanorods are no longer detected in the bloodstream at 1 h post-injection in mice [17]. Hemmer et al. observed the low toxicity of Gd(OH)$_3$ nanoparticles and proposed that the attraction between the oxhydriles of the surface and aqueous cell media may contribute to biocompatibility [46].

Moreover, coating can also contribute to the stability and biocompatibility of the nanoparticles. The studies performed with Mag@Gd(OH)$_3$@Man showed that the coating stabilized the hybrid nanoparticle system, since lower leaching of gadolinium ions was observed compared with uncoated samples. This is in agreement with the work of Shabanzadeh-Kouyakhi, who reported that by using dextrose as a capping agent, the toxicity of gadolinium can be suppressed [41]. The stability of the nanohybrid system is important not only for toxicity issues but also for achieving reliable results in MRI. If the gadolinium hydroxide is leached from the nanoparticles, the accumulation could be different to the behavior of magnetic iron oxide, hampering the dual diagnosis by MRI. Mannose seems to help in the stabilization of hybrid nanoparticles, at least in in vitro experiments.

5. Conclusions

A nanohybrid material composed of magnetite and gadolinium hydroxide was synthesized for the first time, to the best of the authors' knowledge. Although the formation of a core–shell structure with an iron oxide core and a gadolinium hydroxide shell was not achieved, the information provided by the multiple characterization techniques gave sufficient evidence for the formation of a coupled bi-component system. In general terms, the sum of all techniques reveals the hybrid nature of Mag@$Gd(OH)_3$ with suitable properties to be potentially used as a CA. It was observed that the resulting nanosystem preserves its superparamagnetic behavior after modification with the paramagnetic compound.

The further mannose coating was successfully implemented, generating a novel platform that has not been proposed before, to the best of the authors' knowledge. On the basis of the stability studies, it could be said that uncoated hybrid nanoparticles were less stable than mannose-coated nanohybrids. Therefore, the incorporation of a coating is of vital importance for further biological application. Nonetheless, the treatment with FBS can also stabilize the hybrid nanoparticles, as established in the Discussion section.

The results reported in this work are the first stage required for the validation of nanohybrids as dual CAs for MRI, as explored in our previous works.

Supplementary Materials: The following supporting information can be downloaded from https://www.mdpi.com/article/10.3390/colloids7010008/s1, a pdf file containing Figure S1: TEM image of Mag@$Gd(OH)_3$@Man; Figure S2 UV-Vis spectroscopy of the supernatant of stability assays and Figure S3: FTIR of Mag@$Gd(OH)_3$ and Mag@$Gd(OH)_3$@Man after the stability assays. The original TEM images of all the nanoparticles synthesized in this work can be also found in supplementary Material.

Author Contributions: Conceptualization, M.G.M.S. and V.LL.; Methodology, P.S.R. and M.G.M.S.; Investigation, P.S.R. and M.G.M.S.; Data analysis, P.S.R., G.A.M.M. and M.G.M.S.; Supervision, F.H.S. and V.L.L.; Funding acquisition, F.H.S. and V.L.L.; Writing—original draft, M.G.M.S. and V.L.L.; Writing—review and editing, M.G.M.S., G.A.M.M., F.H.S. and V.L.L. All authors have read and agreed to the published version of the manuscript.

Funding: This work received financial support of CONICET, ANPCyT (grants PICT-Start up-2018-00058, PICT 2018 3476.) and Universidad Nacional del Sur (PGI UNS 24-ZQ09). Partial financial support was received of CONICET grant 11220200102280CO, Universidad Nacional de La Plata (grant PID 11 × 897) and PICT 2017-1748 (grant PICT 2017-1748).

Data Availability Statement: Not applicable.

Acknowledgments: Authors thank CONICET, ANPyT, Universidad Nacional del Sur and Universidad Nacional de La Plata for the financial support.

Conflicts of Interest: The authors declare no conflict of interest.

References

1. Wahsner, J.; Gale, E.M.; Rodríguez-Rodríguez, A.; Caravan, P. Chemistry of MRI contrast agents: Current challenges and new frontiers. *Chem. Rev.* **2019**, *119*, 957–1057. [CrossRef] [PubMed]
2. Forte, E.; Fiorenza, D.; Torino, E.; Di Polidoro, A.C.; Cavaliere, C.; Netti, P.A.; Salvatore, M.; Aiello, M. Radiolabeled PET/MRI Nanoparticles for Tumor Imaging. *J. Clin. Med.* **2020**, *9*, 89. [CrossRef] [PubMed]
3. Thomsen, H.S. Nephrogenic systemic fibrosis: A serious adverse reaction to gadolinium-1997-2006-2016. Part 1. *Acta Radiol.* **2016**, *57*, 515–520. [CrossRef] [PubMed]
4. Jeon, M.; Halbert, M.V.; Stephen, Z.R.; Zhang, M. Iron Oxide Nanoparticles as T1 Contrast Agents for Magnetic Resonance Imaging: Fundamentals, Challenges, Applications, and Prospectives. *Adv. Mater.* **2021**, *33*, e1906539. [CrossRef]
5. Raymond, K.N.; Pierre, V.C. Next generation, high relaxivity gadolinium MRI agents. *Bioconjug. Chem.* **2005**, *16*, 3–8. [CrossRef]
6. Mortezazadeh, T.; Gholibegloo, E.; Alam, N.R.; Dehghani, S.; Haghgoo, S.; Ghanaati, H.; Khoobi, M. Gadolinium (III) oxide nanoparticles coated with folic acid-functionalized poly(β-cyclodextrin-co-pentetic acid) as a biocompatible targeted nano-contrast agent for cancer diagnostic: In vitro and in vivo studies. *Magn. Reson. Mater. Phys. Biol. Med.* **2019**, *32*, 487–500. [CrossRef]
7. Dai, Y.; Wu, C.; Wang, S.; Li, Q.; Zhang, M.; Li, J.; Xu, K. Comparative study on in vivo behavior of PEGylated gadolinium oxide nanoparticles and Magnevist as MRI contrast agent. *Nanomed. Nanotechnol. Biol. Med.* **2018**, *14*, 547–555. [CrossRef]

8. Sousa, F.; Sanavio, B.; Saccani, A.; Tang, Y.; Zucca, I.; Carney, T.M.; Mastropietro, A.; Jacob Silva, P.H.; Carney, R.P.; Schenk, K.; et al. Superparamagnetic nanoparticles as high efficiency magnetic resonance imaging T2 contrast agent. *Bioconjug. Chem.* **2017**, *28*, 161–170. [CrossRef]
9. Thapa, B.; Diaz-Diestra, D.; Beltran-Huarac, J.; Weiner, B.R.; Morell, G. Enhanced MRI T 2 Relaxivity in Contrast-Probed Anchor-Free PEGylated Iron Oxide Nanoparticles. *Nanoscale Res. Lett.* **2017**, *12*, 312. [CrossRef]
10. Pellico, J.; Ruiz-Cabello, J.; Fernández-Barahona, I.; Gutiérrez, L.; Lechuga-Vieco, A.V.; Enríquez, J.A.; del Morales, M.P.; Herranz, F. One-step fast synthesis of nanoparticles for MRI: Coating chemistry as the key variable determining positive or negative contrast. *Langmuir* **2017**, *33*, 10239–10247. [CrossRef]
11. Montiel Schneider, M.G.; Lassalle, V.L. Magnetic iron oxide nanoparticles as novel and efficient tools for atherosclerosis diagnosis. *Biomed. Pharmacother.* **2017**, *93*, 1098–1115. [CrossRef] [PubMed]
12. Estelrich, J.; Sánchez-Martín, M.J.; Busquets, M.A. Nanoparticles in magnetic resonance imaging: From simple to dual contrast agents. *Int. J. Nanomed.* **2015**, *10*, 1727–1741. [CrossRef]
13. Shin, T.H.; Choi, Y.; Kim, S.; Cheon, J. Recent advances in magnetic nanoparticle-based multi-modal imaging. *Chem. Soc. Rev.* **2015**, *44*, 4501–4516. [CrossRef] [PubMed]
14. Duan, B.; Wang, D.; Wu, H.; Xu, P.; Jiang, P.; Xia, G.; Liu, Z.; Wang, H.; Guo, Z.; Chen, Q. Core-Shell Structurized Fe_3O_4@C@MnO_2 Nanoparticles as pH Responsive T1-T2∗ Dual-Modal Contrast Agents for Tumor Diagnosis. *ACS Biomater. Sci. Eng.* **2018**, *4*, 3047–3054. [CrossRef] [PubMed]
15. Bao, J.; Guo, S.; Zu, X.; Zhuang, Y.; Fan, D.; Zhang, Y.; Shi, Y.; Pang, X.; Ji, Z.; Cheng, J. Magnetic vortex nanoring coated with gadolinium oxide for highly enhanced T1-T2 dual-modality magnetic resonance imaging-guided magnetic hyperthermia cancer ablation. *Biomed. Pharmacother.* **2022**, *150*, 112926. [CrossRef]
16. Huang, S.; Liu, J.; Liu, D.; Yuan, Q. Facile and large-scale synthesis of $Gd(OH)_3$ nanorods for MR imaging with low toxicity w. *N. J. Chem.* **2012**, *36*, 1335–1338. [CrossRef]
17. Yang, Y.; Sun, Y.; Liu, Y.; Peng, J.; Wu, Y.; Zhang, Y.; Feng, W.; Li, F. Biomaterials Long-term in vivo biodistribution and toxicity of $Gd(OH)_3$ nanorods. *Biomaterials* **2013**, *34*, 508–515. [CrossRef]
18. Montiel Schneider, M.G.; Martín, M.J.; Coral, D.F.; Muraca, D.; Gentili, C.; Fernández van Raap, M.B.; Lassalle, V.L. Selective contrast agents with potential to the earlier detection of tumors: Insights on synthetic pathways, physicochemical properties and performance in MRI assays. *Colloids Surfaces B Biointerfaces* **2018**, *170*, 470–478. [CrossRef]
19. Amiri, H.; Bordonali, L.; Lascialfari, A.; Wan, S.; Monopoli, M.P.; Lynch, I.; Laurent, S.; Mahmoudi, M. Protein corona affects the relaxivity and MRI contrast efficiency of magnetic nanoparticles. *Nanoscale* **2013**, *5*, 8656. [CrossRef]
20. Kang, J.G.; Min, B.K.; Sohn, Y. Synthesis and characterization of $Gd(OH)_3$ and Gd_2O_3 nanorods. *Ceram. Int.* **2015**, *41*, 1243–1248. [CrossRef]
21. Ullah, N.; Imran, M.; Liang, K.; Yuan, C.Z.; Zeb, A.; Jiang, N.; Qazi, U.Y.; Sahar, S.; Xu, A.W. Highly dispersed ultra-small Pd nanoparticles on gadolinium hydroxide nanorods for efficient hydrogenation reactions. *Nanoscale* **2017**, *9*, 13800–13807. [CrossRef] [PubMed]
22. Stoia, M.; Istratie, R.; Păcurariu, C. Investigation of magnetite nanoparticles stability in air by thermal analysis and FTIR spectroscopy. *J. Therm. Anal. Calorim.* **2016**, *125*, 1185–1198. [CrossRef]
23. Chen, F.; Zhang, X.H.; Hu, X.D.; Zhang, W.; Zeng, R.; Liu, P.D.; Zhang, H.Q. Synthesis and characteristics of nanorods of gadolinium hydroxide and gadolinium oxide. *J. Alloys Compd.* **2016**, *664*, 311–316. [CrossRef]
24. Lim, J.; Yeap, S.; Che, H.; Low, S. Characterization of magnetic nanoparticle by dynamic light scattering. *Nanoscale Res. Lett.* **2013**, *8*, 381. [CrossRef] [PubMed]
25. Jin, R.; Lin, B.; Li, D.; Ai, H. Superparamagnetic iron oxide nanoparticles for MR imaging and therapy: Design considerations and clinical applications. *Curr. Opin. Pharmacol.* **2014**, *18*, 18–27. [CrossRef] [PubMed]
26. Honary, S.; Barabadi, H.; Ebrahimi, P.; Naghibi, F.; Alizadeh, A. Development and optimization of biometal nanoparticles by using mathematical methodology: A microbial approach. *J. Nano Res.* **2015**, *30*, 106–115. [CrossRef]
27. Caciandone, M.; Niculescu, A.G.; Roșu, A.R.; Grumezescu, V.; Negut, I.; Holban, A.M.; Oprea, O.; Vasile, B.; Ștefan; Bîrcă, A.C.; et al. PEG-Functionalized Magnetite Nanoparticles for Modulation of Microbial Biofilms on Voice Prosthesis. *Antibiotics* **2021**, *11*, 39. [CrossRef]
28. Sathya, A.; Kalyani, S.; Ranoo, S.; Philip, J. One-step microwave-assisted synthesis of water-dispersible Fe3O4 magnetic nanoclusters for hyperthermia applications. *J. Magn. Magn. Mater.* **2017**, *439*, 107–113. [CrossRef]
29. Kaur, G.; Sharma, P.; Priya, R.; Pandey, O.P. Thermal dehydration kinetics involved during the conversion of gadolinium hydroxide to gadolinium oxide. *J. Alloys Compd.* **2020**, *822*, 153450. [CrossRef]
30. Nadeem, K.; Ali, L.; Gul, I.; Rizwan, S.; Mumtaz, M. Effect of silica coating on the structural, dielectric, and magnetic properties of maghemite nanoparticles. *J. Non. Cryst. Solids* **2014**, *404*, 72–77. [CrossRef]
31. Muscas, G.; Concas, G.; Cannas, C.; Musinu, A.; Ardu, A.; Orrù, F.; Fiorani, D.; Laureti, S.; Rinaldi, D.; Piccaluga, G.; et al. Magnetic properties of small magnetite nanocrystals. *J. Phys. Chem. C* **2013**, *117*, 23378–23384. [CrossRef]
32. Kopac, T. Protein corona, understanding the nanoparticle–protein interactions and future perspectives: A critical review. *Int. J. Biol. Macromol.* **2021**, *169*, 290–301. [CrossRef] [PubMed]
33. Cavalu, S.; Simon, V. Proteins adsorption to orthopaedic biomaterials: Vibrational spectroscopy evidence. *J. Optoelectron. Adv. Mater.* **2007**, *9*, 3297–3302.

34. Dalle Vedove, E.; Costabile, G.; Merkel, O.M. Mannose and Mannose-6-Phosphate Receptor–Targeted Drug Delivery Systems and Their Application in Cancer Therapy. *Adv. Healthc. Mater.* **2018**, *7*, 1701398. [CrossRef] [PubMed]
35. Wang, S.; Zhou, Y.; Liang, T.; Guo, X. Catalytic pyrolysis of mannose as a model compound of hemicellulose over zeolites. *Biomass Bioenergy* **2013**, *57*, 106–112. [CrossRef]
36. Barrera, G.N.; Piloni, R.V.; Moldenaers, P.; Iturriaga, L.B.; Ribotta, P.D. Rheological behavior of the galactomannan fraction from Gleditsia triacanthos seed in aqueous dispersion. *Food Hydrocoll.* **2022**, *132*, 107848. [CrossRef]
37. Siva Kumar, D.; Chandra Babu Naidu, K.; Mohamed Rafi, M.; Prem Nazeer, K.; Ayisha Begam, A.; Ramesh Kumar, G. Structural and dielectric properties of superparamagnetic iron oxide nanoparticles (SPIONs) stabilized by sugar solutions. *Mater. Sci. Pol.* **2018**, *36*, 123–133. [CrossRef]
38. Azcona, P.L.; Montiel Schneider, M.G.; Grünhut, M.; Lassalle, V.L. Stimuli-responsive nanotheranostics intended for oncological diseases:: In vitro evaluation of their target, diagnostic and drug release capabilities. *New J. Chem.* **2019**, *43*, 2126–2133. [CrossRef]
39. Kumar, P.; Khanduri, H.; Pathak, S.; Singh, A.; Basheed, G.A.; Pant, R.P. Temperature selectivity for single phase hydrothermal synthesis of PEG-400 coated magnetite nanoparticles. *Dalt. Trans.* **2020**, *49*, 8672–8683. [CrossRef]
40. Nicolás, P.; Saleta, M.; Troiani, H.; Zysler, R.; Lassalle, V.; Ferreira, M.L. Preparation of iron oxide nanoparticles stabilized with biomolecules: Experimental and mechanistic issues. *Acta Biomater.* **2013**, *9*, 4754–4762. [CrossRef]
41. Shabanzadeh-Kouyakhi, A.; Masoudi, A.; Ardestani, M. Synthesis method of novel Gd_2O_3@Fe_3O_4 nanocomposite modified by dextrose capping agent. *Ceram. Int.* **2020**, *46*, 13442–13448. [CrossRef]
42. Fajaroh, F.; Setyawan, H.; Nur, A.; Lenggoro, I.W. Thermal stability of silica-coated magnetite nanoparticles prepared by an electrochemical method. *Adv. Powder Technol.* **2013**, *24*, 507–511. [CrossRef]
43. García-Soriano, D.; Milán-Rois, P.; Lafuente-Gómez, N.; Navío, C.; Gutiérrez, L.; Cussó, L.; Desco, M.; Calle, D.; Somoza, Á.; Salas, G. Iron oxide-manganese oxide nanoparticles with tunable morphology and switchable MRI contrast mode triggered by intracellular conditions. *J. Colloid Interface Sci.* **2022**, *613*, 447–460. [CrossRef] [PubMed]
44. Janko, C.; Zaloga, J.; Pöttler, M.; Dürr, S.; Eberbeck, D.; Tietze, R.; Lyer, S.; Alexiou, C. Strategies to optimize the biocompatibility of iron oxide nanoparticles–"SPIONs safe by design". *J. Magn. Magn. Mater.* **2017**, *431*, 281–284. [CrossRef]
45. Azcona, P.; López-Corral, I.; Lassalle, V. Fabrication of folic acid magnetic nanotheranostics: An insight on the formation mechanism, physicochemical properties and stability in simulated physiological media. *Colloids Surfaces A Physicochem. Eng. Asp.* **2018**, *537*, 185–196. [CrossRef]
46. Hemmer, E.; Kohl, Y.; Colquhoun, V.; Thielecke, H.; Soga, K.; Mathur, S. Probing cytotoxicity of gadolinium hydroxide nanostructures. *J. Phys. Chem. B* **2010**, *114*, 4358–4365. [CrossRef] [PubMed]